Generalized phase-matching conditions for high harmonics: The role of field-gradient forces

Philippe Balcou,[1] Pascal Salières,[2] Anne L'Huillier,[3] and Maciej Lewenstein[2]

[1] *Laboratoire d'Electronique Quantique–Physique des Lasers,*
Unité Mixte de Recherches 6627, Centre National de la Recherche Scientifique,
Université de Rennes 1, Campus de Beaulieu, F-35042 Rennes, France
[2] *Service des Photons, Atomes et Molécules, Bâtiment 522, Centre d'Etudes de Saclay,*
Commissariat à l'Energie Atomique, F-91191 Gif-sur-Yvette, France
[3] *Department of Physics, Lund Institute of Technology,*
P.O. Box 118, S-221 00 Lund, Sweden
(Received 3 December 1996)

We present an approach to describe the phase matching of high harmonics emitted by laser driven atoms in a nonperturbative regime, for which the atomic response displays an intrinsic intensity-dependent phase. We show that the traditional phase-matching conditions involving conservation of wave vectors should be modified by taking into account the gradient of this atomic phase. We investigate various focusing geometries and interpret the numerical results of Salières *et al.* [Phys. Rev. Lett. **74**, 3776 (1995)]. Within the framework of the two-step model, we demonstrate that the gradient of the intensity-dependent phase can be considered as the canonical momentum gained by the electron in the continuum due to acceleration by field-gradient forces, including in particular the ponderomotive force. [S1050-2947(97)07704-4]

PACS number(s): 42.65 Ky, 32.80 Rm

I. INTRODUCTION

When an intense short laser pulse is focused into an atomic gas medium, extremely high harmonics can be generated [1,2]. In spite of numerous studies devoted to this phenomenon, some of its characteristics are not yet fully understood. The aspect of phase matching is specially challenging: weak-field, perturbative theories fail completely to describe how high harmonics are generated, because of the nonperturbative character of the atomic response. Almost all nonperturbative atomic models of high harmonic generation predict in particular that harmonics are not in phase with the laser, but exhibit phase shifts that depend strongly on the laser intensity. These phase variations have been shown to affect strongly the angular distributions of the emitted harmonic field [3–6]. Salières *et al.* [7] have studied recently the influence of the intrinsic phases on the spatial, temporal, and spectral coherence properties of high harmonics. In this paper, we generalize the traditional phase-matching conditions to the strong-field regime, taking such intrinsic phases into account. In the framework of the recently proposed two-step model for harmonic generation [8–10], we show that field-gradient effects, and in particular ponderomotive force effects, are absolutely essential to assure momentum conservation of the coupled atom-laser and harmonic field system. This situation may thus be termed a novel *dynamical* regime for phase matching.

The paper is organized as follows. In Sec. II, we present in detail the two-step model; in particular we discuss the phases of individual atomic dipoles and their intensity dependences from a point of view of Feynman's interpretation of quantum mechanics [11]. The atomic dipoles are represented here as sums of contributions from different quantum paths, and each of the contributions carries a phase related to the classical action along the corresponding path. In Sec. III, we discuss the physical role of the individual phases in

propagation and phase matching. Here, we derive the basic results of the present paper by applying the stationary phase method to the total phase of the (nonlinear) atomic polarization (composed of the individual dynamically induced phase and the contribution due to the phase of the fundamental laser beam). This leads to the derivation of *generalized phase-matching conditions*. In Sec. IV, we compare our analytical results with the numerical results of Refs. [7,12]. Finally, Sec. V contains a discussion of the physical meaning of the generalized phase-matching conditions; we interpret these conditions in terms of field-gradient forces, and discuss their role in maintaining momentum conservation in the coupled laser-atom-harmonic field system.

II. THE TWO-STEP MODEL AND THE DYNAMICALLY INDUCED PHASES

The origin of intrinsic phases can be best understood within the framework of the so-called two-step model [8–10]. In this semiclassical approach, the electron first tunnels through the Coulomb potential barrier lowered by the slowly varying laser electric field, at some time t_i. The subsequent motion in the continuum is considered as that of a free electron in the laser field. If the electron returns to the vicinity of the ionic core, it may recombine and emit a burst of light at time t_f. This process yields a plateau of high harmonics (with photon energies up to the sum of the ionization potential and of the maximum kinetic energy of the electron), which ends up by a sharp cutoff.

This two-step scenario can be recovered in the fully quantum-mechanical approach of Lewenstein *et al.* [10], as a quasiclassical limit. In the quantum description, however, one takes directly into account the quantum effects of interference, wave packet spreading, and tunneling. In particular one can represent the qth Fourier component of the atomic dipole moment as a sum over quantum paths [13] (to be

consistent with Ref. [10], we use rescaled units throughout for which the electron charge and mass and the velocity of light are $e = m = c = 1$) :

$$\boldsymbol{x}_q = \lim_{t \to \infty} i \int_t^{t + 2\pi/\omega} \exp(iq\omega t_f) dt_f \int_0^{t_f} dt_i \int d^3\boldsymbol{p}$$

$$\times \boldsymbol{d}^*(\boldsymbol{p} - \boldsymbol{A}(t_f)) a^*(t_f) \exp\left(-\frac{i}{\hbar} S(\boldsymbol{p}, t_f, t_i)\right)$$

$$\times \boldsymbol{E}(t_i) \cdot \boldsymbol{d}(\boldsymbol{p} - \boldsymbol{A}(t_i)) a(t_i), \tag{1}$$

where $a(t)$ is the ground state amplitude, $\boldsymbol{A}(t)$ the vector potential, $\boldsymbol{d}(\boldsymbol{p})$ is the dipole moment of the field-free ground-continuum transition, and $\boldsymbol{E}(t)$ the electric field. In the above expression $S(\boldsymbol{p}, t_f, t_i)$ is the *quasiclassical action* for an electron born in the laser field at t_i with a canonical momentum $\boldsymbol{p}$, and returning to the origin at t_f (return time $\tau = t_f - t_i$),

$$S(\boldsymbol{p}, t_f, t_i) = \int_{t_i}^{t_f} dt'' \left(\frac{[\boldsymbol{p} - \boldsymbol{A}(t'')]^2}{2} + I_p\right). \tag{2}$$

We call the action quasiclassical because it contains, in addition to the integral of the kinetic energy, a term proportional to the ionization potential I_p, which determines a potential barrier through which the electron tunnels. The above expression can clearly be interpreted in Feynman's spirit as an integral over all possible electronic trajectories characterized by t_i, t_f, and $\boldsymbol{p}$.

Using a saddle-point analysis, it can be shown that, in the quasiclassical limit, the integral over all possible paths becomes a sum over *relevant* paths, where the relevant paths are determined by the principle of stationary action [12]. This principle thus determines specific values of t_i, t_f, and $\boldsymbol{p}$ (denoted in the following p_{st}). For a given harmonic component in the plateau region of the spectrum, two particular quantum paths (each being associated to a classical trajectory) give the dominant contributions to the dipole moment: one with a return time $\tau_1 = t_f - t_i$ rather short with respect to the optical period, and one with a return time τ_2 almost equal to one optical period. The dipole moment at the harmonic frequency is the coherent sum of amplitudes associated to these quantum paths. Since typically both contributions are comparable (although the second one is slightly larger), their sum exhibits dramatic quantum interference effects.

The phase of each component results from the phase acquired by the electron wave function in the continuum, and from the phase due to the time delay between the recombination time t_f and the reference time of the laser period. It reads [12]

$$\Phi_{at} = q\omega t_f - \frac{1}{\hbar} S(p_{st}, t_i, t_f), \tag{3}$$

where q stands for the harmonic order, ω for the laser angular frequency, and $S(p_{st}, t_i, t_f)$ for the semiclassical action in momentum space along the stationary action trajectory considered [10]. p_{st} is the stationary action value of the canonical momentum of the electron for which the trajectory starting from the atomic core at time t_i returns to it at time t_f.
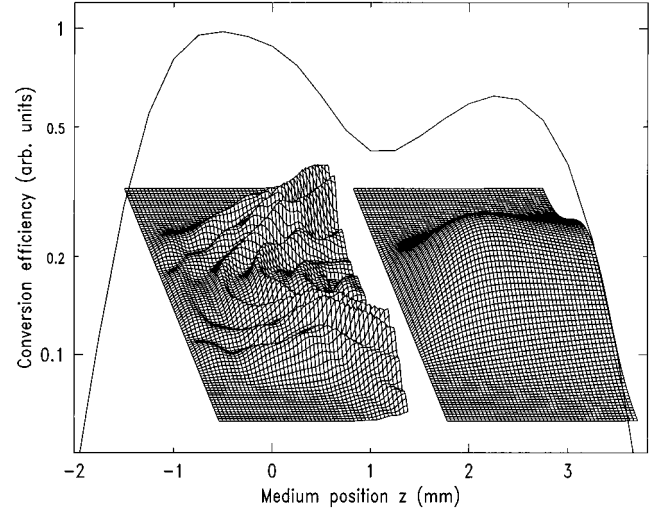

FIG. 1. Conversion efficiency for the 45th harmonic (arb. units) as a function of the position of the center of the medium z, at a peak intensity of 6×10^{14} W/cm^2. The 3D plots show how the harmonic field is constructed in the medium at $z = -1$ mm (left) and $z = 3$ mm (right). The field $|E_q(r,z)|$ (vertical axis) is plotted as a function of z (horizontal axis) and r (direction perpendicular to the plane of the figure). Reproduced from Ref. [7].

For each quantum path, the action can be roughly approximated by $-\tau_s U_p$ (where τ_s is the return time and $U_p = E^2/4\omega^2$ is the ponderomotive potential), and hence decreases linearly with intensity [12]. The return time τ_s has an almost constant value as long as the intensity is low enough for the harmonic to belong to the cutoff region, and switches rather abruptly to another almost constant value at higher intensities, for which it belongs to the plateau. The intrinsic phase thus varies piecewise linearly with the intensity.

Experimentally, high harmonics are generated by focusing an intense laser pulse in a gas jet. The intensity distribution in the focal volume results in a spatial distribution of intrinsic phases, which was shown by Salières *et al.* [7] to have a major impact on how the harmonic builds up in the gas medium. Figure 1, reproduced from Ref. [7], shows how the harmonic yield depends on the medium position z relative to laser focus, for the 45th harmonic of a 825-nm laser, generated in neon with a confocal parameter $b = 5$ mm. Without intrinsic phases, this curve would be symmetric [5,14]. Taking intrinsic phases into account yields a markedly asymmetric curve, with two clear maxima at $z = -1$ mm, and $z = +3$ mm. How the harmonic is generated at these maxima is presented in the insets of Fig. 1. The laser propagates from left to right along the horizontal z axis at the center of the figure. When the gas jet is positioned after the laser focus ($z = 3$ mm), the field is constructed on axis with a smooth, Gaussian-like envelope. On the contrary, when the gas jet is located before the focus, the harmonic is constructed off axis, with an annular structure. Strangely enough, the outgoing harmonic field then turns out to be divergent, even though the laser field is convergent at that point. These phenomena have been explained in [7,15] in terms of variations of the total polarization phase. In the following section, we propose an interpretation based on wave-vector conservation.

III. GENERALIZED PHASE-MATCHING CONDITIONS

In order to interpret this behavior, we consider how the harmonic fields generated at different points are matched in phase. For the sake of clarity, we neglect in the following the dispersion effects due to the linear atomic polarizability, and due to ionization, i.e., due to free electrons and ions. Thus we take the modulus of the wave vector at the harmonic frequency to be $k_q = q\omega/c$ throughout the medium. Note, however, that other effects, e.g., dispersion, could also be included in the theory.

Optimal phase matching will be obtained in direction $\boldsymbol{k}_q$ in a region of space if the harmonic fields generated at any two points $\boldsymbol{r}_1$ and $\boldsymbol{r}_2$ interfere constructively:

$$\arg[P_q(\boldsymbol{r}_1)\exp(i\boldsymbol{k}_q\cdot(\boldsymbol{r}_2-\boldsymbol{r}_1))]=\arg[P_q(\boldsymbol{r}_2)], \quad (4)$$

where P_q stands for the qth Fourier component of the atomic polarization in the medium. It is proportional to the atomic density and to the corresponding Fourier component of the atomic dipole moment as given by Eq. (1). For $\boldsymbol{r}_1$ and $\boldsymbol{r}_2$ close enough, this results in

$$\boldsymbol{k}_q = \nabla\arg(P_q), \quad (5)$$

where the right-hand side represents the polarization wave vector. For incident plane waves and with harmonics generated in a perturbative regime, the phase of the polarization is just q times that of the incident plane wave $\exp(ik_1z)$, so that one obtains the standard condition for perfect phase matching in the forward direction: $k_q = qk_1^0$, with $k_1^0 = \omega/c$. In our case, two other phase factors are involved: the intrinsic, intensity-dependent phase (discussed in the preceding section), and the phase induced by focusing of the fundamental beam (known as the Gouy phase on axis [16]). According to Eq. (5), the phase-matching condition now involves the spatial derivative of all these phases. Let us consider them in turn. The Gouy phase for a Gaussian beam can be expressed as

$$\Phi_{\text{foc}}(r,z) = \arg\left[\frac{1}{b+2iz}\exp\left(-\frac{k_1^0 r^2}{b+2iz}\right)\right]. \quad (6)$$

We use here cylindrical coordinates (r,z), and b stands for the confocal parameter. The total wave vector $\boldsymbol{k}_1$ for the fundamental Gaussian beam is therefore space dependent and reads

$$\boldsymbol{k}_1(r,z) = k_1^0 \boldsymbol{e}_z + \nabla\arg\left[\frac{1}{b+2iz}\exp\left(-\frac{k_1^0 r^2}{b+2iz}\right)\right], \quad (7)$$

where $\boldsymbol{e}_z$ is the unit vector in the z direction.

Second, we characterize the spatial dependence of the atomic phase by means of an effective wave vector $\boldsymbol{K}$ such that

$$\boldsymbol{K}(r,z) = \nabla\Phi_{\text{at}}(r,z), \quad (8)$$

so that condition (5) for optimum phase matching becomes

$$\boldsymbol{k}_q = q\boldsymbol{k}_1 + \boldsymbol{K}. \quad (9)$$

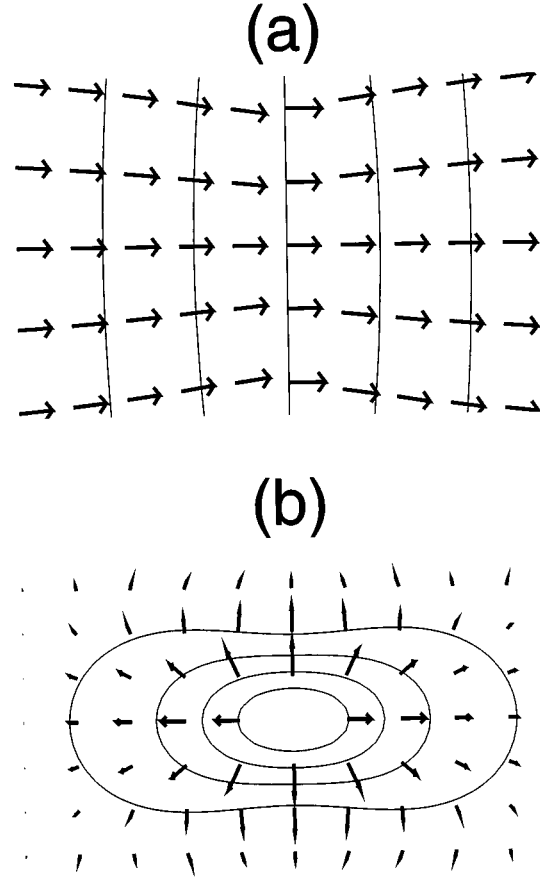Figure 2 shows typical maps of the Gaussian beam wave

FIG. 2. (a) Distribution of the laser beam wave vector $\boldsymbol{k}_1$, taking focusing into account. (b) Distribution of the effective atomic phase wave vector $\boldsymbol{K}$ in the focal region.

vector $\boldsymbol{k}_1(r,z)$ [Fig. 2(a)] and of the effective atomic wave vector $\boldsymbol{K}(r,z)$ [Fig. 2(b)] in the focal region. The laser axis is horizontal at figure center, and the laser pulse is assumed to propagate from left to right. As expected, $\boldsymbol{k}_1$ is mostly directed along the z direction, converges towards the focal point for $z<0$, and diverges for $z>0$. In contrast, $\boldsymbol{K}$ points at a direction opposite to the focal point, yielding a star pattern. As a result of these very different distributions, the way these wave vectors combine differs strongly from point to point near the focus.

Figure 3 shows examples of resulting phase-matching diagrams at different places. For $z=0$ and $r=0$ [Fig. 3(a)], $\boldsymbol{K}=0$ so that one obtains the usual phase mismatch $k_q - qk_1(0,0) = 2q/b$ due to focusing. On the other hand, for points located on axis ($r=0$) and after the focus ($z>0$) [Fig. 3(b)], the effective wave vector $\boldsymbol{K}$ compensates for this focusing phase mismatch, thus realizing collinear phase matching. The harmonic field therefore builds up efficiently close to the axis when the gas jet is placed after the focus.

Conversely, for points located on axis ($r=0$) but before the focus ($z<0$), Fig. 3(c), the effective wave vector $\boldsymbol{K}$ further deteriorates phase matching, so that the harmonic is emitted very inefficiently around those points. However, one can find locations for which noncollinear phase matching is achieved, provided we consider points off axis ($r>0$) and still before the focus ($z<0$). The dashes in Fig. 3(d) repre-
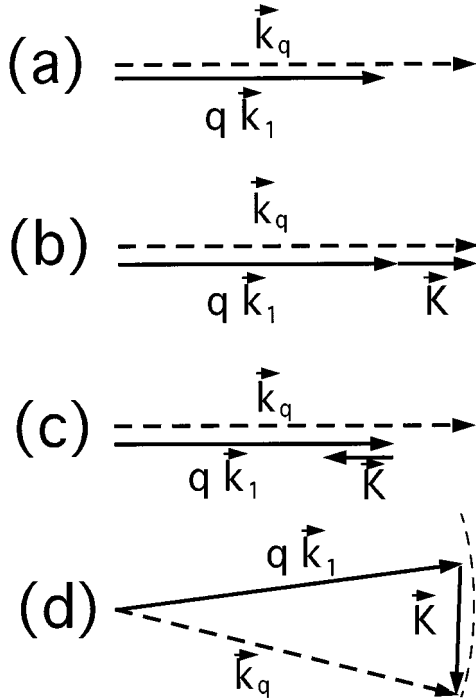
FIG. 3. Examples of phase-matching diagrams arising at different points in the focal region. (a) On axis, exactly at focus; (b) on axis, after the focus: collinear phase matching; (c) on axis, before the focus; (d) off-axis, before the focus: noncollinear phase matching.

sent the locus of k_q (given by $|k_q| = q\omega/c$) in **k** space. The total polarization wave vector $qk_1 + K$ may cross this curve if the negative longitudinal component of **K** remains small, implying that the point remains rather close to focus ($|z| \ll b$.) Such points will form a large ring around the laser axis, yielding an annular structure to the emitted harmonic field. This corresponds to the maximum in the harmonic efficiency at $z = -1$ mm shown in Fig. 1, and explains why the harmonic is generated *off axis* as displayed in the left-hand inset. Moreover, it can be noticed in the example of Fig. 3(d) that the transverse components of qk_1 and k_q are opposite, so that the generated harmonic field may be divergent even though the laser field is convergent. All these qualitative predictions are in agreement with both numerical [7] and experimental results [3]. Of course, perfect phase matching can only be realized at very definite points or curves in the medium. At all other places, condition (5) will not be rigorously fulfilled.

IV. CONTOUR PLOTS OF PHASE MISMATCHES

To investigate in more detail the residual phase mismatches, we introduce a space-dependent mismatch vector field $\delta k(r,z)$, in the direction of $qk_1 + K(r,z)$, and whose norm corresponds to

$$\delta k = k_q - |qk_1 + K|. \tag{10}$$

The harmonic generation will be most efficient when the norm of δk is close to zero, and inefficient otherwise. To get

insights into the distribution of phase mismatches, Fig. 4 shows contour plots of $|\delta k(r,z)|$ in the conditions of Fig. 1. To help the eye, each figure is shaded with a scale from white $[|\delta k(r,z)| = 0]$ to dark grey [large $|\delta k(r,z)|$]. To visualize the direction of harmonic emission, we also represent by arrows the polarization wave vectors $qk_1 + K$. The active medium should be imagined here as a thin slice along the r axis, of typically 1 mm width. The straight dashed lines indicate the center z of the medium in either of the two positions $z = -1$ mm and $z = +3$ mm illustrated in Fig. 1.

As mentioned above, the harmonic phase varies almost linearly with intensity, but with a different slope depending on whether the harmonic is in the cutoff or in the plateau. In the present example, the 45th harmonic phase (in radians) varies as -24.8×10^{-14} I (in W cm^{-2}) in the plateau (for the dominant τ_2-trajectory), and as -13.7×10^{-14} I in the cutoff. The cutoff–plateau transition occurs here at an intensity of 2.3×10^{14} W cm^{-2}. For higher peak intensities, the active medium is separated into a plateau-regime volume, corresponding to the inside of the dot-dashed line on the figures presented, and a cutoff-regime volume farther from focus. In that region, the gradual down slope of laser intensity with increasing distance from focal point results in a major decrease of the harmonic dipole. For this reason, one can expect the harmonic emission to be most efficient either inside the plateau region, or close to the border of the cutoff region.

For the sake of clarity, we first present phase-mismatch distributions using the approximate linear intensity dependence of the atomic phase for the trajectories τ_2 and τ_1 in the plateau regime [Figs. 4(a) and 4(b)], and for the cutoff regime [Fig. 4(c)], assuming a fixed intensity of 6×10^{14} W cm^{-2}. One should therefore keep in mind that, because of this linear approximation, only the distribution inside the dot-dashed line is relevant in Figs. 4(a) and 4(b), and outside this line in Fig. 4(c). For reference, we also plot the phase-mismatch using the phase of the total polarization (i.e., accounting for contributions of all relevant electronic trajectories and interferences among them) in Fig. 4(d).

The different phase-matching configurations described in Figs. 3(a)–3(d) can indeed be found on Fig. 4(a), and are indicated by letters $A-D$, respectively. The most striking feature here is the existence of a large white "walrus-moustache" area for which very good phase-matching is achieved before the focus and off-axis. It connects an on-axis point of collinear phase matching (B) to a large off-axis zone of noncollinear phase matching (D). In the latter region, harmonic emission is indeed mostly divergent; however, it can be noticed that the emission direction changes significantly within these areas, so that the harmonic far-field profile is likely to be far more complex than a simple annular ring, as is again shown by computations and experiments. Left to this white area, the effective wave vector **K** is either insufficient to compensate for the effect of focusing, or even worsens it, so that $|qk_1 + K| < k_q$ (points A and C). On the contrary, **K** overcompensates focusing on the right, so that $|qk_1 + K| > k_q$.

The harmonic can be efficiently generated if both the phase mismatch is small and the medium dimensions are large enough for the field to develop. Positions B and D differ in this respect; the white area is very thin close to B,
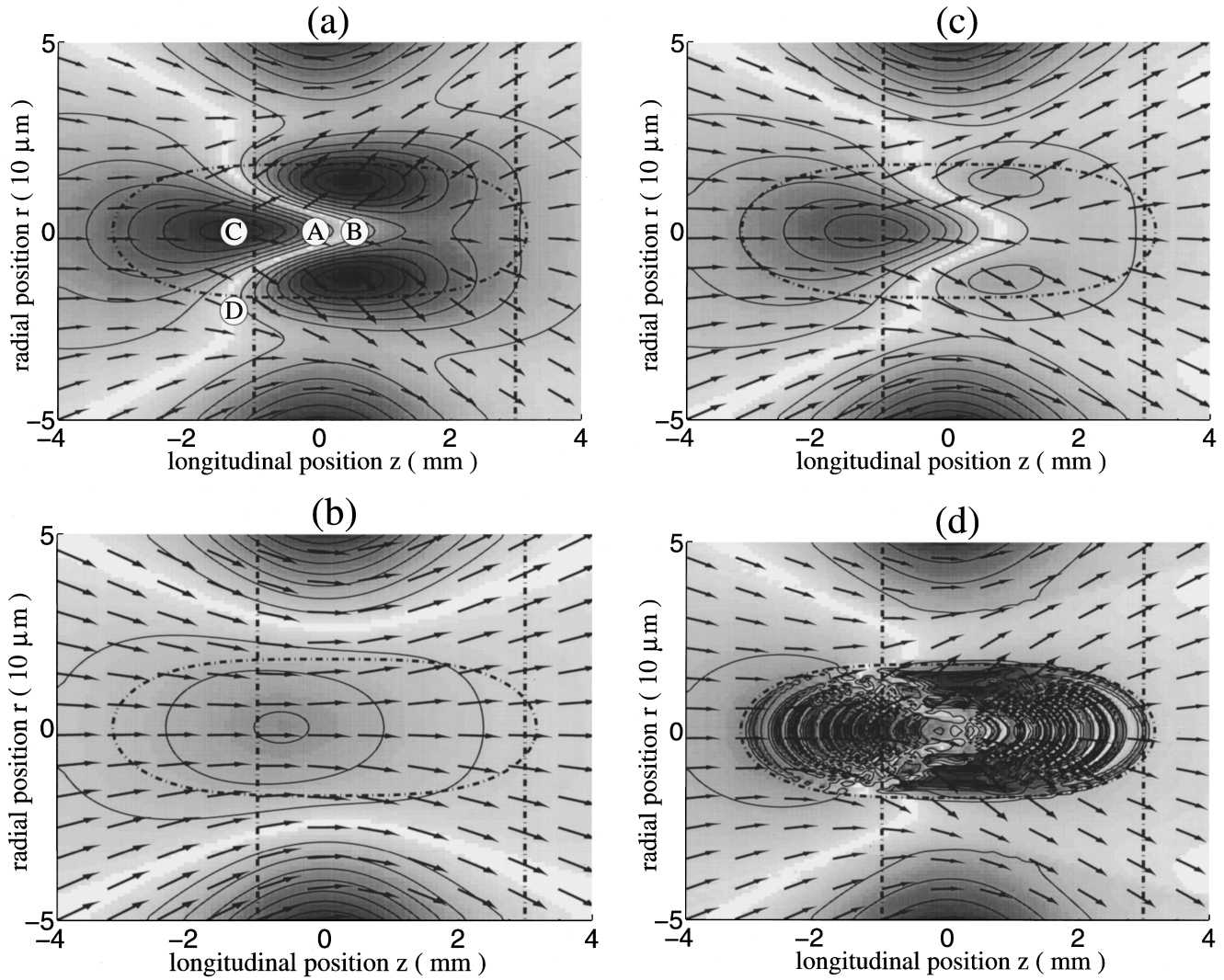
FIG. 4. Contour maps of the phase-mismatch amplitude $|\delta k|$, for different atomic phase variation laws, and in the following conditions: Intensity $I = 6 \times 10^{14}$ W/cm^2, harmonic order $q = 45$, confocal parameter $b = 5$ mm, neon gas. White areas correspond to very good phase matching, dark gray areas to poor phase matching. The arrows represent the resulting directions of harmonic emission. The atomic phase is assumed to vary linearly for the trajectory with the return time τ_2 (a) and τ_1 (b) in the plateau regime, and in the cutoff regime (c). The total phase was used in (d). The cutoff-plateau transition occurs here at 2.3×10^{14} W/cm^2 (dot-dashed line). The relevant area in the focal volume is inside the dot-dashed curve in (a) and (b), and outside in (c). The gas jet positions for maximum harmonic conversion are represented by long dashed lines (at $z = -1$ mm and $z = +3$ mm). In (a), letters A–D indicate the positions at which the phase-matching diagrams of Figs. 3(a)–3(d) occur, respectively.

and much wider around D. Harmonic generation will therefore be most intense in the latter off-axis configuration. By analogy with the notion of spectrally critical or noncritical phase matching used for instance for optical parametric oscillators, one could therefore talk of *spatially critical* phase matching in B, and *spatially noncritical* phase matching in D. Indeed, the position of B is extremely close to the minimum of harmonic conversion seen in Fig. 1, which can be readily related to the two large symmetrical dark areas of poor phase matching at $z = 1$ mm. For even larger z, phase matching is seen to improve significantly, in particular for the trajectory τ_1 [Fig. 4(b)] and even more in the cutoff-regime area shown in Fig. 4(c), which should enhance the conversion efficiency. However, when the medium is displaced to larger z in the cutoff region, the intensity becomes rapidly too low to generate a significant polarization ampli-

tude, so that the harmonic conversion strongly decreases. The emission will hence be most efficient when the medium lies in a compromise position, close to the plateau-cutoff border. This explains qualitatively the origin of the maximum in the harmonic efficiency at $z = 3$ mm shown in Fig. 1. Moreover, the phase mismatch is about constant off axis, or even decreases slightly, so that the field builds up smoothly around the axis, as shown in the right-hand side inset. It is indeed shown in [15] that the resulting harmonic profile is nearly super-Gaussian in these conditions.

It is worth noticing at this point why plotting of the results corresponding to *single* electronic trajectory makes sense. After all, the harmonics are generated by the total atomic polarization, which is a coherent sum of contributions corresponding to all relevant trajectories. Figure 4(d) shows the phase-mismatches distribution arising from the phase of this

total atomic polarization. Clearly the resulting figure lacks the clarity of the previous ones. Due to quantum interference effects, the total phase presents indeed rapid and apparently irregular variations with intensity, which yield complicated contours. As a result, the plot is not so clear to interpret, although the basic structures present in Figs. 4(a)–4(c) are still visible. Moreover, it is obvious from Figs. 4(a)–4(c) that, due to different intensity dependent phases, different contributions will in general propagate in a different manner. In fact, we have recently demontrated that propagation and phase matching may lead to single trajectory selection in the macroscopic signal [17]. In other words, for an appropriately chosen focusing geometry, the macroscopic harmonic signal contains only the contribution of a selected trajectory. Therefore, it is both legitimate and more simple to consider phase mismatches for a single trajectory only.

Introducing contour plots of phase mismatches thus allows us to recover completely the conclusions of Ref. [7], concerning phase-matching in strong fields. However, these results were obtained by numerically integrating the propagation equation, whereas the present *graphical* method does not require extensive calculations. This approach is also completely general and could be applied to any phase-matching problem.

V. PHASE-MATCHING AND FIELD-GRADIENT FORCES

We have introduced so far the effective atomic wave vector **K** as a tool to understand phase matching in strong laser fields. We now wish to stress that it possesses a simple dynamical interpretation in the framework of the semiclassical model. As explained previously and detailed in [12], the dominant term to the atomic phase is proportional to the action of the electron in the continuum, so that its gradient is proportional to the spatial derivative of an action, i.e., a momentum.

To unravel the nature of this momentum, we first calculate the gradient of S and then interpret the result by studying the dynamics of the ionizing electron in the continuum.

Let us first examine the dependence of the semiclassical action S on the atom position x_0. From Eq. (2) , S reads

$$S(x_0,t_i,t_f)=\int_{t_i}^{t_f}\left(I_p+\frac{1}{2}[\boldsymbol{p}_{st}(x_0)-\boldsymbol{A}(x_0,t')]^2\right)dt',$$
(11)

where we have indicated explicitly that both the ''stationary'' momentum $p_{st}=E(x_0)[\cos(t_f)-\cos(t_i)]/(t_f-t_i)$ (i.e., the momentum that allows the electron to return to the core at t_f [10]), and the vector potential $A=-E(x_0)\sin(t)$ now depend on x_0 through the electric field $E(x_0)$. Strictly speaking, the ionization and recombination times t_i and t_f also depend on the electric field amplitude $E(x_0)$. However, it was shown in Ref. [12] that t_i and t_f are actually almost constant, provided the laser intensity is well into either the cutoff or the plateau regime. For simplicity, we will therefore assume throughout that t_i and t_f are constant. Deriving with respect to x_0 yields

$$\hbar\boldsymbol{K}=-\int_{t_i}^{t_f}[\nabla\boldsymbol{p}_{st}(x_0)-\nabla\boldsymbol{A}(x_0,t')]\cdot[\boldsymbol{p}_{st}(x_0)$$

$$-\boldsymbol{A}(x_0,t')]dt'.$$
(12)

We note that the electron velocity $v(t')$ is given by $\boldsymbol{v}(t')=\boldsymbol{p}_{st}-\boldsymbol{A}(t')$, so that this integral contains a vanishing first term $(\nabla\boldsymbol{p}_{st}).\int_{t_i}^{t_f}\boldsymbol{v}(t')dt'$. We have therefore

$$\hbar\boldsymbol{K}=\int_{t_i}^{t_f}\{\nabla\boldsymbol{A}(x_0,t').[\boldsymbol{p}_{st}(x_0)-\boldsymbol{A}(x_0,t')]\}dt'.$$
(13)

This expression can be interpreted if one considers how the electron trajectory and dynamical variables in the spatially varying laser field are perturbed with respect to those in a uniform field. The electron canonical momentum $\boldsymbol{p}$ is no longer a constant of motion, but varies according to the Hamilton equation:

$$\frac{d\boldsymbol{p}}{dt}=-\nabla H^v,$$

$$=(\nabla\boldsymbol{A})\cdot(\boldsymbol{p}-\boldsymbol{A}),$$
(14)

where H^v denotes the velocity gauge Hamiltonian, and the spatial derivatives of A are taken at the electron position $x_0+\delta x(t')$. The typical electron excursion δx with respect to the atom is much smaller than the scale of variation of the laser intensity, so that we can identify A and its derivatives taken at the atom and electron position. We obtain thus

$$\hbar\boldsymbol{K}=\int_{t_i}^{t_f}\frac{d\boldsymbol{p}}{dt}dt'=\boldsymbol{p}(t_f)-\boldsymbol{p}(t_i).$$
(15)

The effective wave vector **K** times $\hbar$ is therefore nothing more than the *canonical* momentum gained by the electron in the continuum.

The origin of the momentum gain can be further ascertained by considering the expression for the action S as given in Ref. [10] for each quantum path:

$$S=(I_p+U_p)\tau_s-2U_p[1-\cos(\tau_s)]/\tau_s$$

$$-U_p[\sin(\tau_s)-4\sin^2(\tau_s/2)/\tau_s]\cos(t_i+t_f).$$
(16)

The dominant contribution to S is just $\tau_s U_p$, so that $\hbar K$ is given to first order as

$$\boldsymbol{p}(t_f)-\boldsymbol{p}(t_i)=(-\nabla U_p(r,z))\tau_s,$$
(17)

where we take advantage of the near-constancy of τ_s in either the cutoff or the plateau regime. The right-hand side is readily seen to be the momentum gained during time τ_s under the effect of a force $-\nabla U_p$, that is, under the ponderomotive force. The next to leading terms to ∇S also depend on the ponderomotive potential gradient ∇U_p, now modulated by an almost periodic function of τ_s and t_f, that vanishes in the deep plateau regime ($\tau_s=2\pi$). The momentum gain $\delta\boldsymbol{P}_{\text{elec}}=\hbar\boldsymbol{K}$ arises therefore from field-gradient forces, dominated by the ponderomotive force.

We can now propose the following quantum interpretation for the effect of the atomic phase on phase-matching. The electron is accelerated in the continuum by field-gradient forces, including in particular the ponderomotive force. When it returns to the ionic core, it has thus gained a

canonical momentum δP_{elec} which is transferred to the harmonic photon, and should be taken into account in the phase-matching condition, now viewed as the momentum conservation equation:

$$\hbar \boldsymbol{k}_q = q\hbar \boldsymbol{k}_1 + \delta \boldsymbol{P}_{\text{elec}}. \tag{18}$$

The momentum of the harmonic photon is thus no longer due solely to the sum of momenta of the incident laser photons, but also to that excess momentum borrowed to the laser beam by the ionizing electron. Of course, as the medium is not of infinite extent, photons can be generated even though this condition is not exactly fulfilled, as is customary for phase matching. A more detailed study is required to ascertain the effect of the finite interaction length, of the spatial variations of the residual phase mismatches, and of the atom momentum.

VI. CONCLUSION

We have proposed an interpretation to phase matching in a nonperturbative regime, for which harmonics display intensity-dependent phases. The gradient of this phase was shown to represent the canonical momentum gained by the electron in the continuum due to field-gradient effects, and in particular to the ponderomotive force. This momentum gain shows up very naturally in the phase-matching condition, viewed as a momentum conservation equation.

We searched how the different wave vectors and the electron momentum gain combine, and unraveled two geometries for which good phase matching is achieved. We find one case of collinear phase-matching, resulting in a smooth Gaussian-like harmonic beam, and one case of noncollinear phase matching, yielding an annular beam. We can thus interpret simply existing numerical calculations and experimental results.

Our approach also explains simply why propagation may select the contribution of only one of the two dominant quantum paths, as shown in [17]. Indeed, the momentum gained by the electron under the effect of field-gradient forces depends on which trajectory it follows. In particular, the momentum gain will be much smaller along the trajectory with a small return time τ_1 than along that with a long return time τ_2. As a result, the phase-matching diagrams also depend on the quantum path. At a specific position in the medium, the generalized phase-matching condition (18) may turn out to be fulfilled for one quantum path only, so that the corresponding contribution will dominate after propagation.

Finally, a basic result of this work is to suggest methods to control the harmonic generation process by inducing suitable perturbations on the electron trajectory. While the canonical momentum acquired by the electron is currently due to the ponderomotive force only, one can also imagine applying inhomogeneous static fields or other laser beams to modify the electron dynamics. This could hopefully stimulate the development of new experimental methods in nonperturbative nonlinear optics.

[1] A. L'Huillier and Ph. Balcou, Phys. Rev. Lett. **70**, 774 (1993).

[2] J. J. Macklin, J. D. Kmetec, and C. L. Gordon III, Phys. Rev. Lett. **70**, 766 (1993).

[3] P. Salières, T. Ditmire, K. S. Budil, M. D. Perry, and Anne L'Huillier, J. Phys. B **27**, L217 (1994).

[4] J. Peatross and D. D. Meyerhofer, Phys. Rev. A **51**, R906 (1995).

[5] J. Peatross, M. V. Fedorov, and K. C. Kulander, J. Opt. Soc. Am. B **12**, 863 (1995).

[6] J. E. Muffet, C.-G. Wahlström, and M. H. R. Hutchinson, J. Phys. B **27**, 5693 (1994).

[7] P. Salières, Anne L'Huillier, and M. Lewenstein, Phys. Rev. Lett. **74**, 3776 (1995).

[8] K. C. Kulander, K. J. Schafer, and J. L. Krause, in *Super-Intense Laser-Atom Physics*, edited by B. Piraux, Anne L'Huillier, and K. Rzazewski, Vol. 316 of NATO Advanced Study Institute Series B: Physics (Plenum Press, New York, 1993), p. 95.

[9] P. B. Corkum, Phys. Rev. Lett. **71**, 1994 (1993).

[10] M. Lewenstein, Ph. Balcou, M. Y. Ivanov, A. L'Huillier, and P. B. Corkum, Phys. Rev. A **49**, 2117 (1994).

[11] R. P. Feynman and A. R. Hibbs, *Quantum Mechanics and Path Integrals* (McGraw-Hill, New York, 1965).

[12] M. Lewenstein, P. Salières, and Anne L'Huillier, Phys. Rev. A **52**, 4747 (1995).

[13] For a review, see Ph. Antoine, M. Gaarde, P. Salières, B. Carré, A. L'Huillier, and M. Lewenstein, in *Proceedings of the VIIth International Conference on Multiphoton Processes*, edited by P. Lambropoulos and H. Walther (Institute of Physics, Bristol, 1997).

[14] Ph. Balcou and Anne L'Huillier, Phys. Rev. A **47**, 1447 (1993).

[15] P. Salières, A. L'Huillier, and M. Lewenstein (unpublished).

[16] See, for example, M. Born and E. Wolf, *Principles of Optics*, 2nd ed. (Pergamon Press, Oxford, 1964), p. 448.

[17] Ph. Antoine, A. L'Huillier, and M. Lewenstein, Phys. Rev. Lett. **77**, 1234 (1996).